



Article

# Proximal Mobile Gamma Spectrometry as Tool for Precision Farming and Field Experimentation

Stefan Pätzold \*, Matthias Leenen and Tobias W. Heggemann †

Institute of Crop Science and Resource Conservation (INRES)—Soil Science and Soil Ecology, University of Bonn, Nussallee 13, 53115 Bonn, Germany; m.leenen@uni-bonn.de (M.L.); tobias.heggemann@lwk.nrw.de (T.W.H.)

\* Correspondence: s.paetzold@uni-bonn.de

† Present address: Chamber of Agriculture North Rhine-Westphalia, Nevinghoff 40, 48147 Münster, Germany.

Received: 29 February 2020; Accepted: 9 May 2020; Published: 14 May 2020



**Abstract:** Soils naturally emit gamma radiation that can be recorded using gamma spectrometry. Spectral features are correlated with soil mineralogy and texture. Recording spectra proximally and in real-time on heterogeneous agricultural fields is an option for precision agriculture. However, the technology has not yet been broadly introduced. This study aims to evaluate the current state-of-the-art by (i) elucidating limitations and (ii) giving application examples. Spectra were recorded with a tractor-mounted spectrometer comprising two 4.2 L sodium iodide (NaI) crystals and were evaluated with the regions of interest for total counts,  $^{40}\text{K}$  Potassium, and  $^{232}\text{Th}$  Thorium. A published site-independent multivariate calibration model was further extended, applied to the data, and compared with site-specific calibrations that relied on linear correlation. In general, site-specific calibration outperformed the site-independent approach. However, in specific cases, different sites could also replace each other in the site-independent model. Transferring site-specific models to neighbouring sites revealed highly variable success. However, even without data, post-processing gamma surveys detected spatial texture patterns. For most sites, mean absolute error of prediction in the test-set validation was below 5% for single texture fractions. On this basis, thematic maps for agricultural management were derived. They showed quantitative information for lime requirement in the range from 1068 to 3560 kg lime  $\text{ha}^{-1} \text{a}^{-1}$  (equivalent to 600–2000 kg calcium oxide (CaO)  $\text{ha}^{-1} \text{a}^{-1}$  if converted to the legally prescribed unit) and for field capacity (26–44%  $v/v$ ). In field experimentation, spatially resolved texture data can serve (i) to optimize the experimental design or (ii) as a complementary variable in statistical evaluation. We concluded that broadening the database and developing universally valid prediction models is needed for introduction into agricultural practice. Though, the current state-of-the-art allows valuable application in precision agriculture and field experimentation, at least on the basis of site-specific or regional basis.

**Keywords:** soil heterogeneity; proximal soil sensing; on-the-go gamma spectroscopy; soil texture; grain size distribution; soil mineralogy; variable rate irrigation; liming; plot trial; precision agriculture

## 1. Introduction

Among diverse non-invasive techniques available, mobile gamma spectrometry (GS) is evolving towards a recognised technology in proximal soil sensing. In the past years, soil scientists have made increasing efforts to evaluate possibilities related to gamma spectrometry and to overcome limitations for practical applications. Proximally recorded gamma spectra provide information on soil properties that are potentially relevant for different applications in agricultural soil use and research [1–3].

Gamma quant emitting radionuclides naturally occur in all soils. Their overlap with current soil properties forms the basis for using gamma spectrometry in soil science and gave rise to multiple studies surveying this relationship. Approximately 90% of the above ground measured gamma radiation

originates from the uppermost 0.3 m of soils, i.e., the main root zone for agricultural crops [4,5]. Relationships between different features of the gamma spectrum (such as total counts, single isotopes or isotope ratios) and sand, silt, and clay contents have been detected in several studies [6–8]. The absolute amounts of radionuclides in a given soil are determined by the local, i.e., site-specific conditions, such as geological, mineralogical, and pedological settings and processes. In the following, this complex of influences is denominated as “geopedological conditions.” One major factor is the mineralogical composition of the soil’s parent material. The sand fraction of European soils is often strongly quartz dominated and, consequently, bears no or very little radionuclides [9,10]. In contrast, the clay fraction is dominated by clay minerals and Fe oxides, both being richer in radionuclides [5,9–11].

Remote GS as well as proximal GS are capable of detecting spatial soil texture patterns at various scales [12,13]. Gamma spectrometry has been proven to perform well on single fields [2], at a very limited number of sites [14], or within geologically homogeneous landscapes [13,15]. Though, for datasets comprising various geopedological conditions, the complexity increases. In this respect, machine learning approaches can be superior to linear correlation models. Support vector machines (SVM) enable calibration of site-independent texture prediction models, overcoming interferences from different parent materials [7,8]. However, to achieve universal applicability in its proper sense, more related studies are needed [3]. In this study, a site-independent model [8] is tested on study sites that were not in the calibration set in order to test its universal applicability.

Mobile gamma measurements can be conducted while driving over the field (on-the-go) or during stationary recordings (stop-and-go) [16]. Both approaches yielded similar results for different soil textures ( $R^2 \geq 0.96$ ; [14]), but must consider that the gamma decay is noisy, i.e., variable over time [17–19]. Some applications of GS such as Digital Soil Mapping (DSM) and management zoning require or profit from data post-processing such as interpolation [12,20]. The same holds true for field experiments on small plots where soil texture is a key soil property with various implications for experimental results [21–23]. In contrast, for agricultural measures, immediate data availability in real-time can be a great advantage; the necessary noise reduction can be done in real time.

Studies that show practical applications in precision agriculture and field experimentation at high spatial resolution are still scarce. In this work, we intend to evaluate the feasibility of highly resolved on-the-go GS to provide quantitative texture-related application data that is currently state-of-the-art.

The aim of this study is to test our published site-independent calibration model [8] for unknown sites in comparison to site-specific calibrations. This evaluation focuses on practical applications in agriculture and field experimentation. Two hypotheses were investigated alongside the chosen case studies: (i) The site-independent model by Heggemann et al. [8] precisely predicts soil texture for unknown sites, and (ii) GS yields soil texture data on-the-go and in real time, i.e., without geostatistical data post processing, at sufficient preciseness for precision agriculture and field experimentation.

## 2. Materials and Methods

### 2.1. Sites and Sample Set

This study comprised five agricultural fields in different regions of Western Germany; two fields in North-Eastern Germany from the precedent study [8] were included only for comparing the calibration approaches (Table 1). A geological map of Germany with the study sites is available in the Figure 1. The soils at the 8-ha Münster field in the North German Plain were developed from Cretaceous marls partially covered by aeolian sand, Saalian fluvial sediments, and glacial till. In the district of Düren, the 8-ha study field was located at the edge of the Rhenish Massif in the Northern Eifel. Here, the soils formed from Pleistocene periglacial slope deposits (PPSD [24]) that consisted of more or less weathered sandstones from the Upper Bunter Sandstone and loess. Texture variability arose from differing PPSD composition and variable degrees of soil erosion in the undulated landscape. Two sites at the Eastern edge of the Eifel (Rhenish Massif) were investigated. First, a field of 2.8 ha size was located in the district of Ahrweiler. Second, in the municipality of Rheinbach, two neighbouring fields were

investigated (Rheinbach-1: cropland, 2.1 ha; Rheinbach-2: permanent pasture, 2.3 ha). At both sites, soils have developed from PPSD composed from variable amounts of intensively weathered Lower Devonian sand, silt- and claystones and loess. The soils in the Uckermark district have developed from Weichselian glacial till on the ground moraine. The Münster, Rheinbach-1, and the two Uckermark (35 and 25 ha) fields had already been part of the precedent study and are described in more detail by Heggemann et al. [8].

**Table 1.** Investigated fields and related soil texture parameters.

Site	Land Use	No. of Soil Samples; Sampling Strategy	Sand Mean Content (min-max) [%] in Conventionally Analysed Soil Samples	Silt	Clay
Münster	Cropland	45 (raster)	57 (21–80)	15 (9–21)	26 (9–55)
Düren	Cropland				
	whole field experimental plots	11 (stratified) 48 (plots)	44 (34–59)	38 (26–44)	16 (11–20)
Ahrweiler	Cropland	71 (raster)	12 (7–23)	57 (37–70)	30 (18–57)
Rheinbach-1	Cropland	42 (raster)	25 (12–37)	43 (40–65)	14 (21–28)
Rheinbach-2	permanent pasture	81 (raster)	38 (22–51)	40 (27–49)	20 (14–28)
Uckermark-1	Cropland	81 (stratified)	61 (36–81)	23 (11–40)	14 (5–21)
Uckermark-2	Cropland	39 (stratified)	57 (34–78)	26 (16–37)	16 (6–27)



**Figure 1.** Set-up for recording gamma spectra stop-and-go as well as on-the-go. The two crystals mounted to the steel frame are positioned 0.3 m above the soil surface. The photomultiplier console and the computer are in the tractor cabin.

Two plot experiments at the sites Düren and Rheinbach-2 were investigated. Within the 8 ha Düren field, a fertilizer experiment with 48 plots of 108 m<sup>2</sup> each had been set up by the Chamber of Agriculture of North Rhine-Westphalia (Germany) prior to the GS survey; that is, the gamma results were not considered for designing that experiment. The example was nevertheless chosen to assess the potential GS support for future design and positioning of plot experiments. The plots covered 5184 m<sup>2</sup>; including the inter-plot spacings, the total area of the experiment comprised 8613 m<sup>2</sup>.

At the pasture of Rheinbach-2, revealing strongly acidified soils, a liming experiment was established after the GS survey in November 2018. Three treatments in threefold repetition were to be

optimally placed in a strip design. The legacy soil map for agriculture 1:5000 [25] suggested area-wide homogeneous soil properties. However, a preliminary on-the-go survey revealed considerable texture heterogeneity. In consequence, the experimental design was modified and treatments were placed in strips of 6 m width that captured as much heterogeneity as possible. Afterwards, raster points were defined and sampled for conventional analyses as well as for capturing liming effects over time with a portable mid-infrared spectrometer (not subject to this study). Another aim of the trial is a long-term survey on grassland vegetation changes. At the raster points, gamma spectra were recorded stop-and-go for model calibration.

## 2.2. Ground Truth Sampling and Soil Analyses

Three different approaches to define sampling points were applied (Table 1). (i) To evaluate gamma performance for soil mapping at the field scale (e.g., as basic information for management zoning), the reference sampling points were selected upon completion of an on-the-go survey in order to cover the whole range of gamma counts at the respective site (stratified sampling). (ii) To elucidate the usefulness of gamma data as basic information for, e.g., lime dosage in precision farming, sampling was conducted along a regular raster with a grid width along the tractor tracks. (iii) Soil samples in the Düren field experiment were taken as composite samples in the centre of each plot. Each reference soil sample was composed of three subsamples and was taken from 0–0.3 m depth with a Pürckhauer drill.

Soil samples were homogenised, air-dried, pestled, and sieved at 2 mm to remove stones. The particle size distribution was determined with the combined sieve and pipette method [26]. Organic matter and, if present, calcium carbonate were removed prior to particle size analysis. The grain sizes were classified, following the World Reference Base for Soil Resources [27], into sand (2000–63  $\mu\text{m}$ ), silt (63–2  $\mu\text{m}$ ), and clay (<2  $\mu\text{m}$ ). Soil survey in Germany utilises the same grain size classes. Texture classes predicted from gamma spectra were adapted to the common scheme of GD-NRW and AG Boden [25,28] to enable direct comparison with legacy soil maps. In this study, (i) lime dosage and (ii) field capacity (FC) are presented as examples for texture-related GS applications in precision farming. For lime dosage, soil texture was translated into the scheme of the Association of German Agricultural Analytical and Research Institutes (VDLUFA); for details, refer to [29]. Field capacity was calculated via pedotransfer functions on the basis of the texture classes used in the German soil survey [28].

## 2.3. Gamma Measurements

### 2.3.1. Principles

Gamma quants are marked by characteristic energy levels, enabling us to identify the causal gamma-ray source. Besides the total gamma counts (TC),  $^{40}\text{Potassium}$  (K-40),  $^{238}\text{Uranium}$  (U-238), and  $^{232}\text{Thorium}$  (Th-232) can be detected by mobile gamma spectrometry directly in the field because these naturally occurring radionuclides reveal a sufficient abundance and energy. To monitor these elements by so called Regions of Interest (ROIs) with defined energies is the common approach, and this is sometimes also denoted as the “windows method.” The ROIs range from 1.37–1.57 MeV for K-40, 1.66–1.86 MeV for U-238, and 2.41–2.81 MeV for Th-232. The ROI for TC ranges from 0.4–2.81 MeV [3]. Due to the attenuation of gamma quants originating from greater depth, gamma data mainly provide information on topsoil [4,5]. An alternative method to evaluate gamma spectra is the Full Spectrum Analysis (FSA) approach that requires more efforts in data post-processing and yields equivalent results [2].

Diverse features of gamma spectra are related to soil texture [6–8]. Two main reasons for more or less pronounced correlations must be considered. First, particle size is directly linked to specific surface area in soil and, thus, to sorption capacity for radionuclides. Second, K-40, U-238, and Th-232 are incorporated in the lattice structure of certain minerals [3]. Nuclide quality and quantity in soil are controlled by the mineralogy and geochemistry of the parent material as well as by geological and

pedogenic processes [3,30,31]. Multiple interactions between mineralogical composition of the parent material, soil texture, and the resulting gamma emission make the interpretation of gamma spectra a complex problem. Particularly diverse weathering processes liberate radionuclides from primary and secondary minerals and submit them to pedogenesis, including redistribution and leaching processes. In this study, the term “geopedological conditions” is used to summarize the complex influence of various geological, mineralogical, and pedological settings and processes. One specific problem in recording gamma spectra originates from the statistical distribution of radioactive decay over time [17]. This noise is relevant during stop-and-go as well as on-the-go gamma recordings [3]. Different pre-processing methods are capable of reducing noise to improve gamma data evaluation [2,18]. However, the simple moving window approach also yielded valuable results [19].

### 2.3.2. Instrumentation and Data Recording

A gamma spectrometer RSX-1 (Radiation Solutions Inc., Mississauga, ON, Canada) was used. The two 4.2 L thallium activated sodium iodide crystals were mounted on a steel frame for the tractor’s three-point linkage to record gamma spectra directly in the field (Figure 1).

The two crystals were coupled to a digital spectrometer console to synchronously process incoming gamma-ray pulses towards a 1024 channel spectrum. Positioning data were provided by an internal GPS module. Field gamma spectra were recorded either stop-and-go or on-the-go, both in an identical geometric measurement setup. All gamma recordings were conducted 0.3 m above soil surface at 1 Hz frequency. On-the-go data were recorded at velocities of 0.7–1.4 m s<sup>-1</sup>, and were adapted to the actual driving conditions on the respective field. Measurement lane spacing for on-the-go data acquisition varied from 6 to 27 m with respect to the tractor tracks on the respective fields. To calibrate models with ground truth data, spectra were taken in stop-and-go mode, i.e., the tractor was stopped at the sampling location and spectra were recorded for 60 sec.

All gamma spectra were evaluated with the commercial RadAssist software (Radiation Solutions Inc., Mississauga, ON, Canada). This program uses the windows approach, i.e., besides the total counts (TC), the Regions of Interest (ROI) for K-40, U-238, and Th-232 were also analysed. For evaluating and displaying spatial data, the ArcGIS software package (v. 10.1, ESRI Inc., Redlands, CA, USA) was used.

### 2.3.3. Noise Reduction

Gamma decay is not deterministic, but reveals statistical uncertainty over time [17], which is also denoted as noise. The variable decay rate as recorded when measuring at 1 Hz rate is exemplary, shown in Figure 2a. However, more sources of uncertainty have to be considered in GS. During on-the-go surveys, data collection at 1 Hz rate when driving at, e.g., 0.7 m s<sup>-1</sup> resulted in 1.4 spectra m<sup>-1</sup> driving distance. The footprint (in the literature also denoted as “support”) is the area from which the signal arises; it has no sharp boundary, but the relative signal contribution decreases with increasing distance between the gamma emitting source and the crystal [3]. For the chosen geometric setting, a single spectrum comes from a footprint with an approximately 2 m radius around the crystals. In consequence, the footprints of neighbored spectra overlap to a significant extent that cannot be specified. Furthermore, recording spectra on-the-go captures not only the variability in decay rates, but also gamma ray emission variability that is related to soil heterogeneity over very small distances.

To cope with the different sources of uncertainty, a moving window approach was applied as a smoothing algorithm for all on-the-go surveys (Figure 2b). This approach was chosen with respect to the linear spectra alignment along the tractor lanes. From five subsequent spectra, the mean values for each ROI were calculated, i.e., each spectrum was considered in five mean values and the total number of measuring points (i.e., spatial data density) was not reduced.

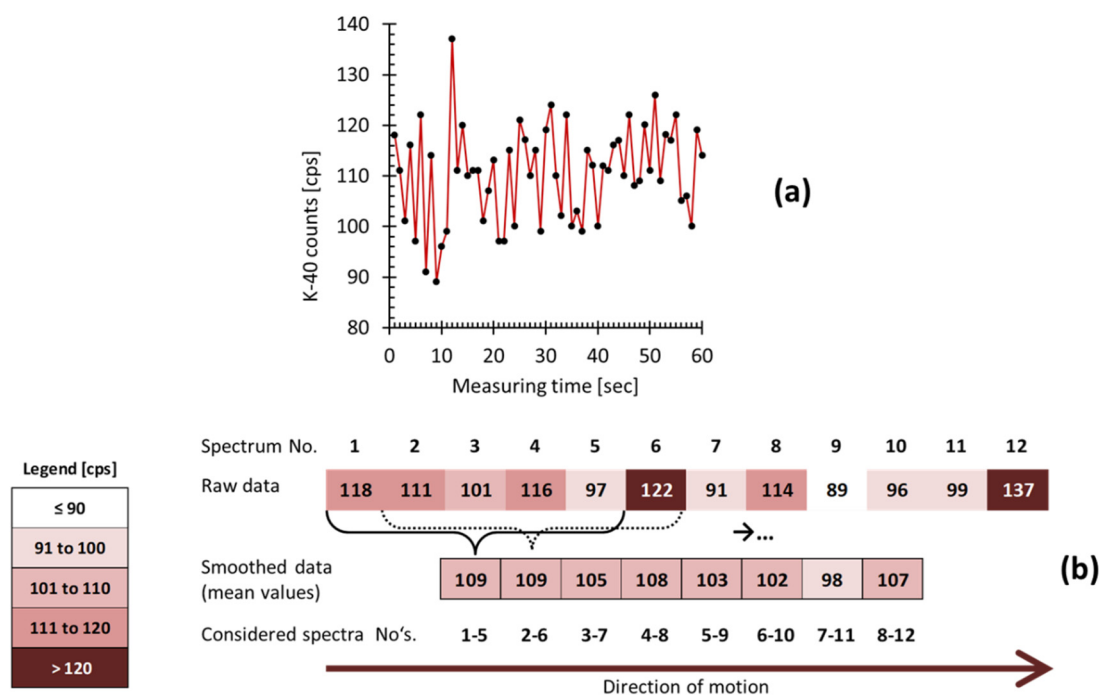


**Figure 2.** (a) Variable decay rates (noise) during a stop-and-go measurement of 60 s at the Düren site, and (b) schematic visualisation of the moving window approach to smooth the noisy data recorded on-the-go (data from Figure 2a).

#### 2.4. Model Calibration

In a precedent study by Heggemann et al. [8], a site-independent model for texture prediction was successfully calibrated using support vector machines (SVM). That study comprised ten sites with largely different geopedological conditions comprising soils from fluvial and aeolian sediments, glacial till, and PPSD. The transferability of the model to unknown sites was to be tested in this study. First, the published model was enlarged by the Ahrweiler dataset, and a model was calibrated as described in the earlier study [8]. The training on the calibration dataset was performed using 100 times 10-fold cross validation in order to find the optimal prediction models (i.e., with the lowest prediction error for sand, silt, and clay). To test model transferability, one site was excluded from the calibration set, and the model was re-calibrated. For validation, the re-calibrated model was applied to the excluded site (test-set validation). Finally, two pairs of fields were selected to evaluate their crosswise substitution: datasets from (i) two sites in the Uckermark district (Weichselian ground moraine), and (ii) the fields Ahrweiler and Rheinbach-1 (Eastern Eifel, Rhenish Massif). In the original model, soils formed from PPSD were represented by 42 samples from the Rheinbach-1 field. This parent material is very frequent in the Rhenish Massif (approx. 25800 km<sup>2</sup>) and prevails also in the Ahrweiler region.

Besides, in this study, site-specific models were tested and compared with the site-independent model. Therefore, linear correlations between gamma features and grain size fractions were calculated for the samples of each field. Site-specific models were trained with 70% randomly selected samples and validated with the remaining 30% of the samples from that site.

In this study, the count rates for the different ROIs as provided by the software were used without further treatment to minimise efforts for data processing in view of the envisaged real-time applications.

### 2.5. Statistical Evaluation

The root mean square error (RMSE) for calibration models, the mean absolute error (MAE) for prediction (test-set validation), and the coefficient of determination were calculated as follows:

$$\text{RMSE} = \sqrt{\frac{1}{n} \sum_{i=1}^n (f_i - y_i)^2} \quad (1)$$

$$\text{MAE} = \frac{1}{n} \sum_{i=1}^n |f_i - y_i| \quad (2)$$

$$R^2 = \frac{\sum_{i=1}^n (f_i - \bar{y})(y_i - \bar{y})}{\sum_{i=1}^n (y_i - \bar{y})^2} \quad (3)$$

where  $f_i$  is the predicted, and  $y_i$  the respective observed value. The RMSE and the MAE were considered acceptable when the respective values were below 5% for the single fractions of sand, silt, and clay.

## 3. Results

### 3.1. Comparing Site-Independent and Site-Specific Calibration

The re-evaluation of the site-independent calibration published by Heggemann et al. [8] revealed that this model was not generally capable of predicting soil texture at sites that were not adequately represented in the calibration set. To evaluate model performance on totally independent sites, single sites were completely removed from the calibration data and the model was then applied to the eliminated site (see Section 2.4). That way, predicting soil texture for Münster led to unacceptable MAEs (i.e., >5%; Table 2). In the original study [8], texture prediction for Münster had been successful with the site-independent model, which was when a subset of the Münster samples were present in the calibration set. However, in this study, the two Uckermark fields could completely replace each other in the calibration dataset. Completely leaving out one of the fields for calibration still led to acceptable prediction error for the remaining field. This result was expected because the two fields were located at only 8.4 km distance and revealed the same geopedological conditions.

**Table 2.** Mean absolute errors for predicting grain size classes (in % of the fine earth) using the support vector machines (SVM)-modelling approach as published by Heggemann et al. [8]. Five separate models were calibrated, leaving out one complete site per model. That site was used for test-set validation to test transferability of the respective model.

Calibration					Validation					Mean Absolute Error [%] for VAL (Prediction)		
CAL Sites (N)	Conventionally Measured Grain Size Classes [%] in CAL Dataset	Conventional Grain Size			VAL Site <sup>(1)</sup> (N)	Conventionally Measured Grain Size Classes [%] in VAL Dataset	Conventional Grain Size			Sand	Silt	Clay
		Sand	Silt	Clay			Sand	Silt	Clay			
2–11 (N = 510)	Min/Max	6/81	11/87	4/57	1 (N = 79)	Min/Max	21/80	9/21	9/55	21	15	15
	Mean	31.1	47.2	20.2		Mean	63.0	14.4	21.2			
	SD	19.5	16.2	6.8		SD	13.2	2.6	10.9			
1 & 3–11 (N = 508)	Min/Max	6/80	9/87	4/57	2 (N = 81)	Min/Max	36/81	11/40	5/21	4	3	3
	Mean	31.1	45.9	21.4		Mean	61.0	23.4	14.0			
	SD	20.4	18.3	7.4		SD	7.4	4.3	3.5			
1–2 & 4–11 (N = 550)	Min/Max	6/81	9/87	4/57	3 (N = 39)	Min/Max	34/78	16/37	6/27	4	3	3
	Mean	33.9	44.0	20.7		Mean	56.9	25.6	16.0			
	SD	21.5	18.8	7.5		SD	9.5	4.8	5.9			
1–3 & 5–11 (N = 547)	Min/Max	6/81	9/87	4/57	4 (N = 42)	Min/Max	12/37	40/65	14/28	5	18	12
	Mean	36.2	42.0	20.3		Mean	24.6	52.8	21.4			
	SD	22.2	19.2	7.7		SD	6.8	7.0	2.7			
1–10 (N = 523)	Min/Max	6/81	9/87	4/55	11 (N = 66)	Min/Max	7/23	37/69	18/57	4	7	7
	Mean	38.4	40.9	19.3		Mean	11.7	57.7	29.1			
	SD	21.2	18.9	6.6		SD	3.7	7.8	7.7			

Abbreviations: VAL = validation, CAL = calibration, MAE = mean absolute error, Min/Max = range, SD = standard deviation. <sup>(1)</sup> Sites: 1 = Münster; 2 = Uckermark-1; 3 = Uckermark-2; 4 = Rheinbach-1; 11 = Ahrweiler; for sites 5–10 that are not under study here, see [8].

In contrast, texture prediction for the Rheinbach-1 and Ahrweiler fields failed if only the respective other field was included in the site-independent calibration ( $MAE > 5\%$ ). The complex composition of PPSD probably impeded a better result. First, the amounts of loess in the PPSD were different, which can be seen from the mean silt contents (Table 2). Second, the PPSD component derived from Lower Devonian sand-, silt-, and claystones revealed varying weathering degree. At Rheinbach, smectite was present, which was not the case at Ahrweiler (one X-ray diffraction (XRD) analysis per field, not shown). These differences probably impeded model transferability between the two sites that were located at only 7.5 km distance and in the same geological landscape. The failure of the site-independent model at the Ahrweiler field was obvious when measured and the predicted clay contents were plotted (Figure 3). However, the local calibration for the clay was performing sufficiently well ( $R^2 = 0.73$ ,  $MAE = 3.5\%$  clay).

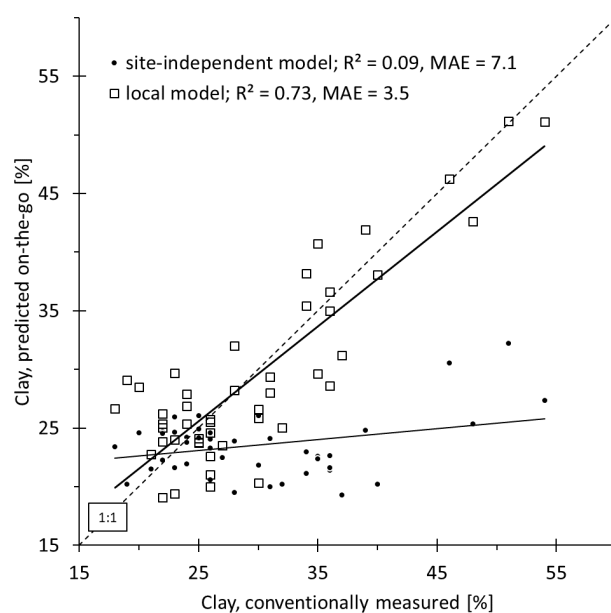


**Figure 3.** Performance of on-the-go clay prediction at the Ahrweiler field with (i) the SVM-based site-independent model [8], originally calibrated on 10 sites, for this study extended by data from the Ahrweiler field, and (ii) a linear local (site-specific) model.

### 3.2. Recognition of Spatial Patterns

At the pasture of Rheinbach-2, the 4666 on-the-go spectra revealed a bimodal frequency distribution (Figure 4a). A clear spatial pattern became obvious when the dataset was separated in two classes at the local minimum of 825 cps (Figure 4b). This data distribution originates from a complex geopedological situation that frequently occurs in the Eifel region. Lower Devonian sedimentary sand-, silt- and claystones (shales) have been folded during the Hercynian orogenesis, forming ridges and troughs [32]. Therefore, sandstone and shale can be found side-by-side within a few meters distance. During the Mesozoic and Tertiary, intensive and deep weathering left behind softened rocks and clay-rich layers. Solifluction during the Pleistocene transported and mixed the weathering products to a certain degree, forming PPSD that are finally the parent material of Holocene soil formation [24]. As could be seen here, the soils still may mirror the character of the underlying rocks.

The legacy soil map, shown as the background in Figure 4b, did not reflect the observed field zones as defined by the TC classes. This was not a simple scale problem as can be seen from even smaller map units (abbreviated by capital letters in the map unit ID) in a close neighbourhood north and east of the studied plot. Topsoil texture was regarded as rather homogeneous by the mapping pedologist (first digit of the map unit ID); the texture class was group 3 with 8–30% clay and >50% silt (clayey silt according to GD-NRW [25]). In fact, conventional laboratory texture analyses ( $N = 109$ )

revealed clay and silt contents from 14 to 28% and from 27 to 49%, respectively, in the north-western part of the plot. A correct classification would consequently have led to the groups 2 (clayey loam), 4 (sandy loam), and 5 (heavy loamy sand).

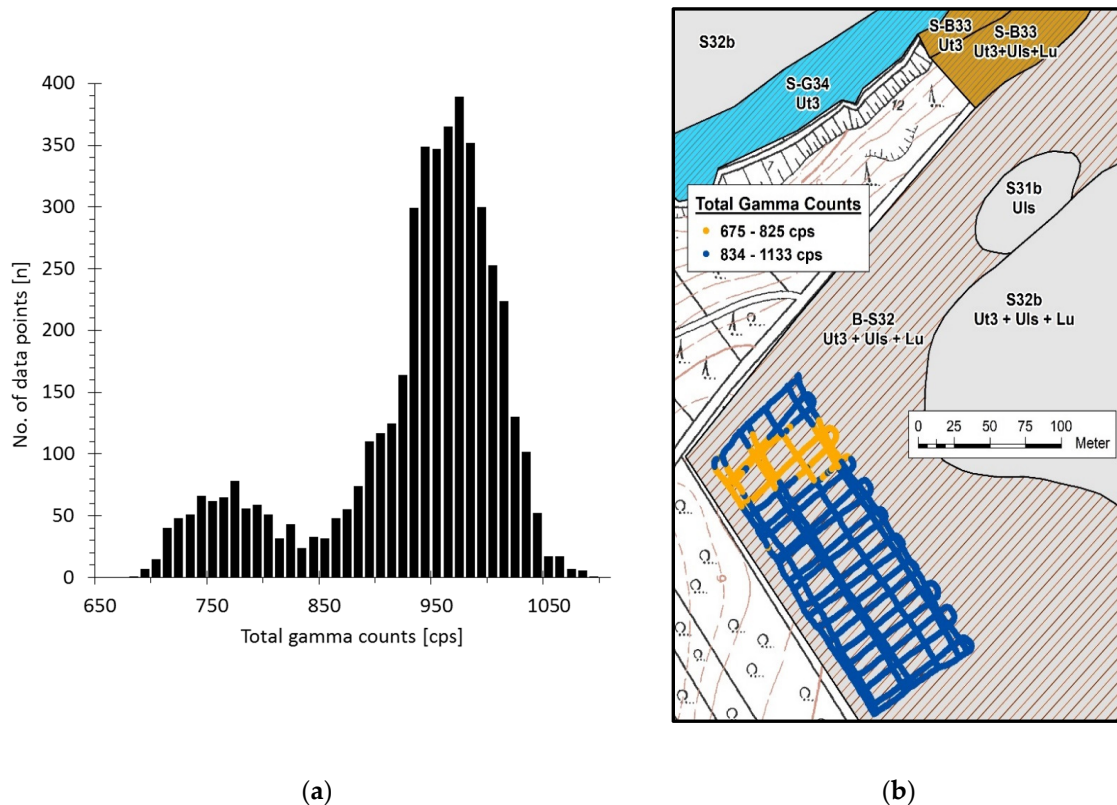


**Figure 4.** (a) Frequency distribution and (b) spatial pattern of the total gamma counts (in orange and blue) on the 2-ha permanent pasture Rheinbach-2 ( $n = 4666$ ). Spectra were recorded on-the-go and smoothed as explained in Section 2.3.3. The background map is the legacy soil map for agriculture 1:5000 [25]; forested areas are not mapped.

### 3.3. Texture Prediction

Figure 5 shows the relationship between clay and gamma TC at the study sites Münster and Ahrweiler. In both cases, TC and clay were closely related, but with opposite orientation. While simple pattern recognition, as shown in Section 3.2, was not concerned by differences in clay mineralogy, this result shows that quantitative texture prediction must take local geopedological conditions into account.

While Münster and Ahrweiler were located at approximately 150 km distance and in different geological landscapes, the three study sites in the Eastern Rhenish Massif (Table 3) were assumed to be similar. However, even within this region, contrasting relationships between the total counts and clay occurred. For the two Rheinbach fields,  $R^2$  for clay prediction was not satisfactory. With respect to the small range of clay contents, this result was not surprising and can further be explained with the landscape relief as discussed below. The negative correlation between clay and the total counts at Ahrweiler correspond to the result presented in Section 3.4.1.

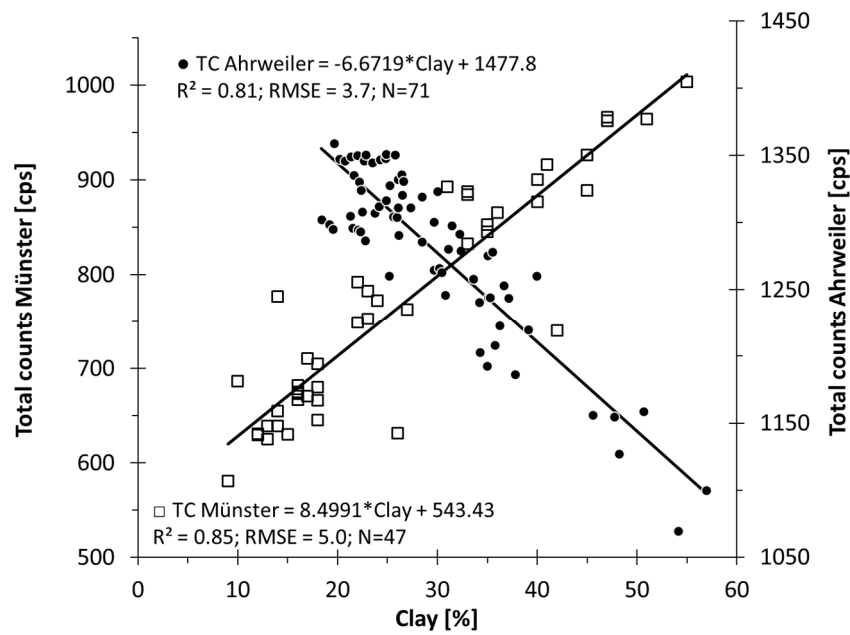


**Figure 5.** Correlation between clay content and total gamma counts (TC) at the study fields Münster and Ahrweiler. Fundamental differences in clay mineralogy led to the contrasting relationship between clay content and TC.

**Table 3.** Relationship between measured clay contents and total gamma counts at three test fields in the Eastern Rhenish Massif.

Site	Clay [%] min-max	Total Counts [cps] min-max	Correlation Equation	R <sup>2</sup>	RMSE	N
Ahrweiler	18–57	1069–1359	TC = −6.7 × clay + 1478	0.81	3.7	71
Rheinbach-1, cropland	14–28	868–1143	TC = −6.3 × clay + 1181	0.06	2.5	42
Rheinbach-2, pasture	14–29	834–1133	TC = 21.6 × clay + 549	0.60	2.2	108

More precise texture information for the two Rheinbach fields was achieved from the correlation between K-40 counts and the sand content (Figure 6).

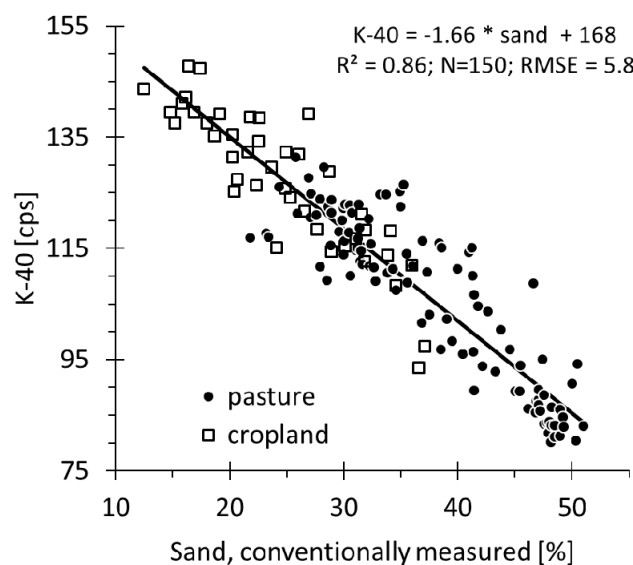


**Figure 6.** Correlation between conventionally measured sand content and K-40 counts for two neighboured pieces of land at Rheinbach (Rhenish Massif).

The correlation equations on the two fields were almost identical when separately calculated (slope -1.68 for the Rheinbach-1 and -1.67 for the Rheinbach-2 field). Therefore, a common model was calibrated for the subsequent sand prediction from on-the-go spectra.

### 3.4. Gamma Spectrometry as a Tool for Precision Farming

Precise texture prediction on-the-go, as shown above, potentially provides options for precision agriculture. The following paragraph gives application examples on how considering site-specific conditions helps to optimize soil management. Therefore, site-specific models were calibrated with the gamma feature that performed best at the respective site.

#### 3.4.1. Considering in-Field Heterogeneity for Estimation of Lime Requirement

For the Ahrweiler field, a clay model was calibrated on the K-40 counts of 48 samples (2/3 of the total sample number;  $\text{Clay} = -0.45 \times \text{K-40 [cps]} + 91$ ). Test-set validation of this model for the predicted clay contents in the remaining 23 samples is shown in Figure 7a. The calibration resulted in  $R^2 = 0.82$  and  $\text{RMSE} = 3.3\%$  clay. Consequently, the model was seen as appropriate for clay prediction on-the-go as illustrated in Figure 7b. Annotation to one of the two clay content classes was correct in most cases. Aberration occurred notably in the transition zone between the areas with large and small clay content; this problem will be discussed below. For the entire field, the mean value of all measured clay contents accounted for 29.5%, while the mean clay content predicted on-the-go accounted for 24.1%. The discrepancy reveals that the large number conventional analyses ( $N = 71$ ) did not match the mean clay content derived from on-the-go spectra ( $N = 2494$ ). Clay content as derived from GS provides a larger spatial information density that is supposed to form a reliable basis for, e.g., lime dosage in precision agriculture.

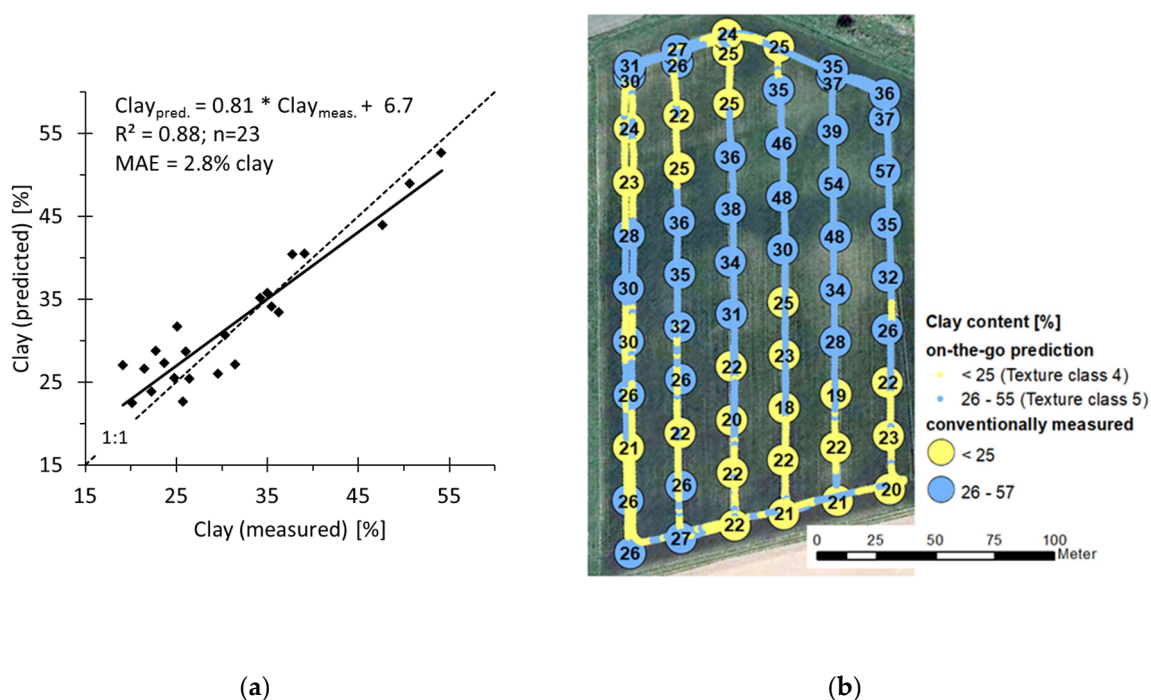


**Figure 7.** (a) Independent test-set validation of clay prediction for the Ahrweiler field (site-specific model calibrated on K-40 counts at 48 sampling points) and (b) field scheme with clay contents along the tractor lanes at the Ahrweiler field as conventionally measured and as predicted from K-40 counts. Small circles along the tractor lanes show the class of clay content predicted on-the-go after calibrating ( $N = 48$ ) and validating ( $N = 23$ ) the site-specific model ( $N = 2494$ ). Numbers in large circles give the conventionally measured clay content at the sampling points. The colours symbolize the annotation to one of the relevant clay content classes [29].

Recommended lime dosage for maintaining optimal pH values depends directly on clay content in the topsoil if organic matter content is below  $40 \text{ g kg}^{-1}$  [29]. Given these premises, Table 4 lists the lime rate for the fields at Ahrweiler and Münster. The two zones of the Ahrweiler field (Figure 7b) should receive 1700 and 2000  $\text{kg CaO ha}^{-1} \text{ a}^{-3}$ , respectively. At Münster, four different lime requirement classes occurred within the field, leading to recommended lime rates within the field ranging from 600 to 1700  $\text{kg CaO ha}^{-1} \text{ a}^{-3}$  (Table 4).

**Table 4.** Management parameters with direct relation to soil texture at the test sites Ahrweiler and Münster. Recommended lime dosage refers to arable soils with optimal pH status and soil organic matter contents  $\leq 40 \text{ g kg}^{-1}$ . Field capacity in undisturbed soil as derived from texture class at low bulk density; water content in pores  $\leq 50 \mu\text{m}$  (n.p. = not predicted because only clay yielded satisfactory prediction).

Clay Content <sup>(1)</sup> [% w/w]	Texture Class According to . . . .		Lime Requirement [kg CaO ha <sup>-1</sup> a <sup>-3</sup> ] <sup>(4)</sup>	Field Capacity [% v/v] <sup>(5)</sup>
	Soil Survey <sup>(2)</sup>	Advisory Service <sup>(3)</sup>		
	Ahrweiler			
45–65	n.p.	5	2000	n.p.
30–45	n.p.	5	2000	n.p.
25–35	n.p.	5	2000	n.p.
17–25	n.p.	4	1700	n.p.
	Münster			
25–45	Lts	4	1700	44
17–25	Ls4	4	1700	39
12–17	Sl4	3	1400	36
8–12	Sl3	2	1000	34
5–8	Sl2	2	1000	28
< 5	Su2	1	600	26

<sup>(1)</sup> Conventionally measured. <sup>(2)</sup> According to [28]: Lts = sandy clay loam, Ls4 = heavy sandy loam, Sl4 = heavy loamy sand, Sl3 = medium loamy sand, Sl2 = light loamy sand, and Su2 = light silty sand. <sup>(3)</sup> According to [29], based solely on the clay content. <sup>(4)</sup> CaO is the legal dimension for lime; conversion to  $\text{CaCO}_3$  by factor 0.7147. <sup>(5)</sup> According to [28].

#### 3.4.2. Estimation of FC as Basic Data for Irrigation Management

At the Münster study site, the geopedological situation was less complex than at Ahrweiler. Therefore, the site-specific model for TC revealed a good correlation with both the sand and clay contents (Sand:  $\text{TC} = -7.5728 \times \text{sand} + 1200.5$  ( $N = 47$ ;  $R^2 = 0.95$ ;  $\text{RMSE} = 3.3$ ); Clay:  $\text{TC} = 8.4991 \times \text{clay} + 543.4$  ( $N = 47$ ;  $R^2 = 0.85$ ;  $\text{RMSE} = 5.0$ ); see Figure 5). In consequence, texture classes and FC—the latter via looking-up tables in the German soil survey handbook [28]—could be derived from on-the-go spectra (Figure 8). For this grid cell map, a mean TC value from all on-the-go spectra within a grid cell was calculated. In other words, each pixel represents the mean value of all spectra recorded in its  $20 \times 20 \text{ m}$  area. No further interpolation or geostatistical data treatment were conducted in view of the aim to provide quantitative texture data on-the-go and in real-time.

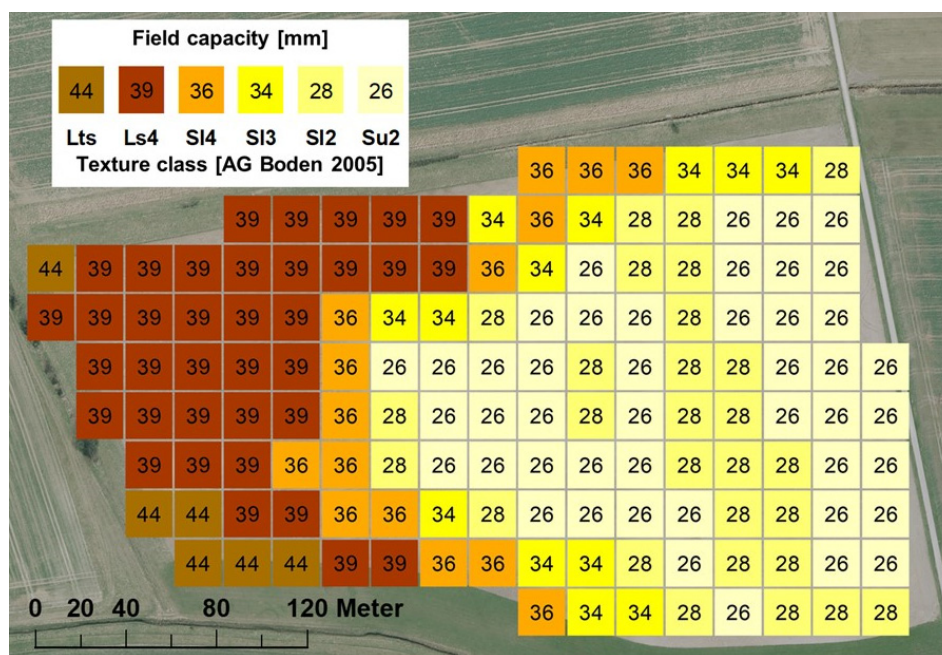


**Figure 8.** Texture classes (represented by different colours) and field capacity (numbers in grid cells, [% v/v]) at the Münster study site as derived from TC recorded on-the-go (Lts = sandy clay loam, Ls4 = heavy sandy loam, SI4 = heavy loamy sand, SI3 = medium loamy sand, SI2 = light loamy sand, and Su2 = light silty sand). Grid cells out of field boundary were cut off.

### 3.5. Gamma Spectrometry as A Tool to Support Field Experimentation

Two running field experiments were selected to demonstrate GS usefulness in field experimentation. In both cases, neither data post-processing (apart from smoothing) nor geostatistical data treatment was conducted.

#### 3.5.1. Choosing the Optimal Position of the Plot Experiment Within the Field

The statistical parameters characterising soil heterogeneity for different positions of the experiment are shown in Table 5. All values rely on a gamma survey of the whole field at 27 m lane spacing. The K-40 measurements were chosen for evaluation of soil heterogeneity because they provided good correlation with soil texture (see Section 3.5.2). The coefficient of variation (CV) for K-40 amounted to 11.2% at the chosen position, while CV for the whole field was 15.1%.

**Table 5.** Statistical parameters for the K-40 counts at the Düren site. The whole field covered an area of 8.0 ha. The plot experiment comprised of 0.86 ha. Small letters indicate significant statistical differences ( $p = 0.005$ ) between four tested positions of the experimental plots (CV = coefficient of variation).

	Whole Field	Realised Position of Experiment	Alternative Positions of Experiment		
			A	B	C
N	3591	256	380	321	360
Min-Max [cps]	86–243	107–189	86–200	96–188	110–181
Mean [cps]	146	146 a	145 a	147 a	141 b
CV %	15.1	11.2	13.2	9.9	9.3

The mean values for the K-40 counts reveal small differences that were, however, significant ( $p = 0.005$ ) between alternative C and the other plot positions. Choosing the positions B or C would have led to smaller coefficients of variation, i.e., to less heterogeneity within the plots, without modifying the plot plan.

### 3.5.2. Supporting Field Experimentation with Texture Prediction at High Spatial Resolution

However, the potential of GS to precisely determine within-field texture heterogeneity can also be utilised at the scale of small experimental plots within a larger field. The chosen plot position of a running experiment on the Düren field (each plot of 108 m<sup>2</sup> size) was evaluated with respect to texture heterogeneity. Based on randomly selected soil samples from 12 of the plots and the respective on-the-go K-40 values (averaged over the plots), model calibration revealed satisfactory correlation between K-40 counts and clay and sand contents, respectively, despite the small sample number (measured clay (%) =  $0.181 \times \text{K-40(cps)} - 11.3$ ;  $R^2 = 0.65$ , RMSE = 1.3; measured sand (%) =  $-0.521 \times \text{K-40(cps)} + 119$ ;  $R^2 = 0.88$ , RMSE = 3.4). Subsequent test-set validation performed well for clay and sand in the remaining 36 plots (Figure 9).

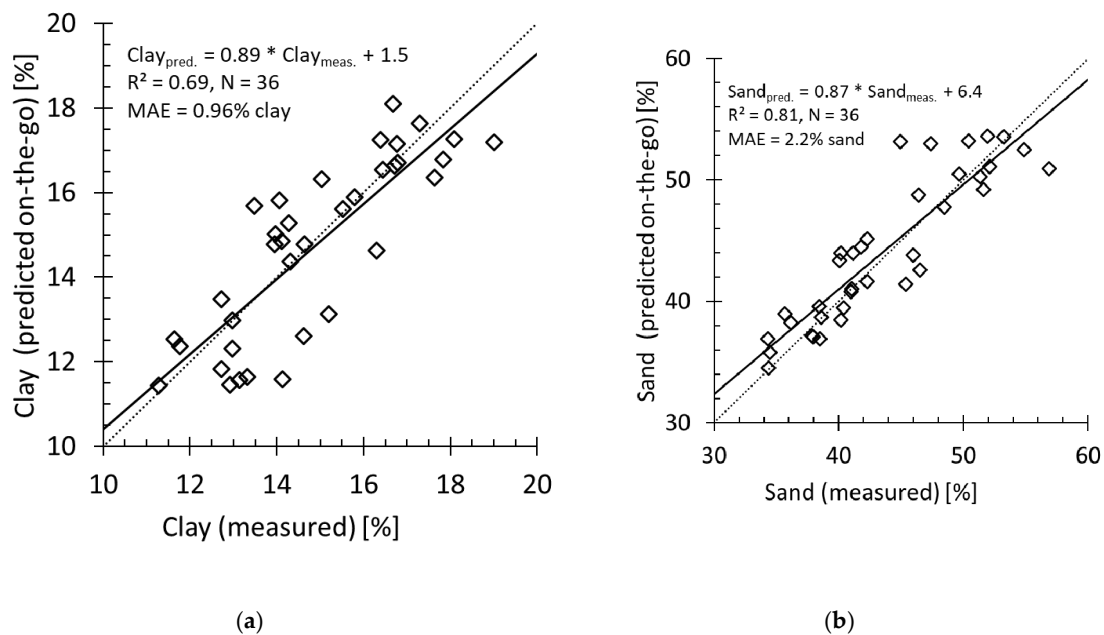


**Figure 9.** On-the-go prediction (test-set validation) for (a) clay and (b) sand contents in small experimental plots at the Düren field. The dotted lines are the 1:1 lines.

From predicted clay and sand content (for prediction error, refer to MAE, Figure 9), silt was calculated. This allowed the derivation of soil texture class according to AG Boden [28] for each single gamma point and for all plots. Figure 10 shows the texture classes as predicted on-the-go (small circles) in comparison to the conventionally measured values in classical composite samples of the 48 experimental plots.

With small efforts for conventional analyses ( $n = 12$ ), valuable data on soil texture class in the entire experiment were derived. This comprehensive information can be used as a co-variable for future statistical evaluation.

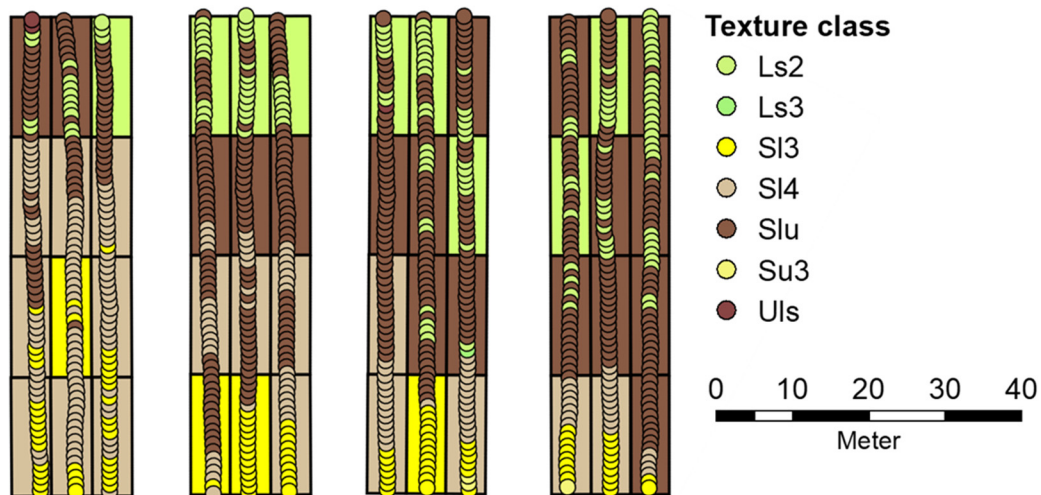


**Figure 10.** Scheme of the running plot experiment Düren. Small circles show predicted soil texture class for all data points of the on-the-go gamma survey. For prediction error, see Figure 9. The background colour in each plot shows the conventionally measured texture class in a composite sample of the respective plot.

### 3.5.3. Providing Texture Information as Co-Variable for Future Vegetation Monitoring in a New Experiment

Figure 11 shows the spatial coincidence between stop-and-go K-40 counts and sand contents at the grid points at the study site Rheinbach-2. The negative correlation reflects the geopedological situation; the sand fraction is dominated by quartz grains originating from the underlying sedimentary sandstone [9,32] that is part of the PPSD. Test-set-validation with 30% of the sample set yielded reliable sand prediction (MAE = 3.1% sand). High spatial resolution of texture information allowed us to establish a dense sampling raster that captured the entire span of sand content variation as already presented in Table 1.

Finally, the most heterogeneous part of the plot was selected on the basis of the TC map (Figure 4) in order to capture as much texture variability as possible.

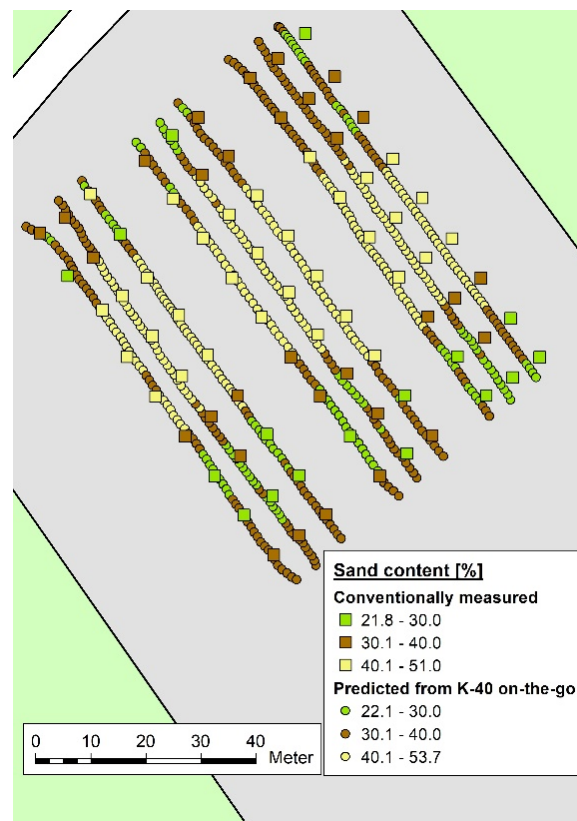


**Figure 11.** Plan of the Rheinbach-2 (pasture) experimental sub-plot. The model shown in Figure 6 was used to predict sand content from the on-the-go spectra (coloured circles). The rectangles show the conventionally measured sand content at 81 out of the 150 sampling points.

## 4. Discussion

### 4.1. Universal Applicability of the Site-Independent Model by Heggemann et al. [8]

This study revealed clear evidence that the site-independent calibration model proposed by Heggemann et al. [8] cannot be considered universally valid. Texture was not precisely predicted for sites with geopedological conditions that were not adequately represented in the calibration set. In such cases, site-specific calibration (i.e., model building directly on the respective site) outperformed the site-independent model. Geographic distance and attribution to a distinct geological map unit are important criteria, but not decisive. This became obvious with the two exemplary site pairs. The site-independent model revealed good transferability between the two Uckermark fields. In contrast, transferability was poor for the fields at Rheinbach and Ahrweiler that were located at only a 7.5 km distance and in the same geopedological region. Minor differences in mineralogical composition of the parent material, weathering degree, and/or the accessory presence of smectite inhibited a better result. Accordingly, van der Klooster et al. [13] reported that models can successfully be transferred between plots or even regions as long as the surveyed soils reveal similar geopedological conditions. Van der Klooster et al. [13] as well as Coulouma et al. [33] state that, in most cases, Th-232 yielded the best correlation to clay content. When the geopedological conditions within the survey differ, more complex relationships between gamma features and soil texture arise, and other gamma features yield best results [8]. Soils developed from PPSD, like in Ahrweiler and Rheinbach, often reflect the very complex geopedological conditions leading to their formation. Previous studies have shown the potential of machine learning algorithms to integrate complex input data in one model [7,8]. In the cases shown here, linear site-specific models still outperformed the site-independent SVM model. Deep insight into geopedological conditions, at least in landscapes with complex parent material and

soil genesis, it is necessary to build appropriate calibration sets. However, a truly universal model is still desirable to further reduce efforts and costs of gamma surveys.

#### *4.2. Recognition of Spatial Patterns of Gamma Features*

This study revealed the relevance of on-the-go gamma spectrometry for practical application in precision agriculture. In that branch, data availability in real-time during on-the-go gamma surveys is an interesting option. When ROIs are displayed while driving or immediately after the survey, spatial soil patterns become readily visible. This makes rapid decisions possible concerning soil mapping, definition of sampling points, or management zone margins. For such applications, quantitative spectra evaluation is not mandatory, and sophisticated data processing steps [2,12] are dispensable. However, depending on the geopedological context, different spectral features may show optimal correlation with soil texture [14,33,34]. Therefore, if only pattern recognition is required, TC as stand-alone proxies are sufficient and, at the same time, less prone to errors than single ROI.

#### *4.3. Quantitative Texture Prediction: Chances and Limitations*

Rapid and precise topsoil texture estimation is possible via GS as shown for some examples in this study. The MAE was generally in the same range as the laboratory inaccuracy for conventional texture analyses [35]. Between the different sites and site-specific models, the prediction error (MAE) varied. The same applies to the contribution of noise (see Figure 2) to the overall uncertainty of the method. Elucidation of these methodological problems requires and merits more in-depth studies.

At Münster, the close positive correlation between TC and the clay content (Figure 5) matched the expectations as reported in literature [13–16]. In this region, the sand fraction in the prevalent glaciofluvial Saalian sediments is dominated by quartz and, consequently, reveals very low TC, while the clay fraction is dominated by montmorillonite and illite [36]. Under such conditions, the abundance of radionuclides depends to a major extent on the clay content. In contrast, at the Ahrweiler site, the clay fraction likely contained kaolinite as described for soils in this region [24]. This two-layer clay mineral reveals very small K contents with respect to its lattice structure and small cation exchange capacity. In consequence, the close negative correlation between clay and TC (Figure 5) is plausible. It is assumed that directly under the sampled loess-containing Ap horizon, the proportion of kaolinite increased. This was probably the reason for the prediction offset in the transition zone between loamy and clayey soils at Ahrweiler. In general, ground truth samples can never exactly reflect the depth the gamma signals were captured from, because it is not precisely delimited. This result again showed that layered soils as well as soils from PPSD must be carefully regarded when planning and evaluating gamma surveys.

Spatial variability of soils and their parent material is often related to the landscape position, notably in periglacial regions [24]. The variable PPSD composition impacted the performance of GS at the two Rheinbach fields (Table 3). The cropland covered the steeper centreslope and footslope while the grassland was located at the more or less flat hilltop. This went along with a dominating loess proportion in the PPSD at the lower landscape positions and a larger proportion of weathered Devonian rocks in the higher positions.

#### *4.4. Application Examples in Precision Agriculture and Field Experimentation*

Precision agriculture: as far as possible, we refrained from geostatistical operations (e.g., interpolation) as proposed in the digital soil mapping approach. Here, the aim was to evaluate the suitability of mobile GS for texture prediction on-the-go that was as unadulterated as possible using suitable reference data for validation. Geostatistical processing can lead to distortions that are not causally related to the gamma data or the related predictions. Of course, gamma data and predictions can undergo further geostatistical processing afterwards [12,15].

On the basis of validated quantitative texture prediction, application examples were presented. Variable rate liming is a recognised approach in precision agriculture that bears economic potential [37];

beyond that, agronomic benefits such as crop health or nutrient availability that are linked to soil pH must be considered [38]. For liming purposes, the detailed texture classes according to the soil survey handbook [28] as shown for Münster are not mandatory because the handbook of fertiliser advisory services [29] classifies only clay contents. In the example from Ahrweiler, the mean value of the measured clay contents of the entire field accounted for 29.5%, while the predicted mean was 24.1% (N = 2494). Uniform liming following the standard approach, i.e., a representative composite soil sample and conventional texture analysis, would consequently have led to lime over-dosage on large parts of the field. If pH values are known to be outside the recommended range, other sensing approaches than GS are advantageous for variable rate liming, but they still require soil sampling [39] or a separate tractor-driven work step [40]. Future lime or fertiliser dosage algorithms could leave behind wide texture classes; instead, stepless recommendations with regard to continuously predicted texture could be developed [39]. However, GS is not capable of directly detecting pH or available nutrients. Therefore, GS should be combined with sensors such as mid-infrared spectrometers that yield nutrient data or related proxies [39,41].

At the Münster study, field geopedological conditions allowed us to predict not only clay, but also sand content. Therefore, texture classes and, via pedotransfer functions [28], FC were derived. Field capacity is considered in irrigation management to adapt water amounts; related maps are, therefore, requested in precision irrigation management [42–44]. Water application that exceeds FC leads to unproductive seepage losses [43]. In the same way as FC, plant available water (PAW) can easily be derived from the texture class [28,44]. However, techniques to map soil hydraulic properties in high resolution are scarce [42]. Other sensing approaches than GS to delineate variable-rate irrigation-zones, namely EMI, provide meaningful information as reviewed by Hagverdi and Leib [42]. An advantage of the presented GS approach is that it yields values for the FC of the topsoil as needed for irrigation management in shallow rooting crops (e.g., potatoes, vegetables). Further, GS is not disturbed by metallic irrigation devices in the vicinity of the sensor.

Field experimentation: two case-studies for implementing GS-based texture information into field experimentation were demonstrated. Reducing unexplained variance is mandatory to optimise the output of cost-intensive field experiments. In this respect, soil texture is a key soil property with implications for, e.g., soil hydrology, organic matter content, nutrient supply, and crop and weed growth. This has been proven by several studies, revealing coincident patterns of soil properties and biomass [21], grain yield [22], or weed patterns [23]. Introducing environmental data into a dataset and enhancing the statistical power during statistical evaluation of a plot experiment can even be realised a-posteriori. The Düren example showed that additional and precise data on soil texture can be provided at the plot scale with reduced analytical effort. Further, GS can help to find the optimal emplacement of a plot experiment within a larger field. Choosing another position for the plots would have minimised the unexplained variance in the statistical evaluation of the Düren experiment. In consequence, rapid on-the-go gamma recordings prior to deciding upon the final plot position can contribute to better experiment results.

At the stage of planning or designing a field experiment, pattern recognition without data post-processing may be sufficient. In the Rheinbach-2 liming experiment, selecting the most heterogeneous part of the field gave a chance to increase the expected output with respect to the specific aims and hypotheses of the trial. Species composition of the grassland sward and changes of mid-infrared spectra will be monitored at the large number of observation points over time. In the Rengen grassland experiment [45] with similar soil properties, 61.7% of the species composition were explained by soil properties and 62% by different fertilisation [45]. Close interaction between changes in grassland species distribution and soil are expected at the Rheinbach-2 field as well. Most probably, maximising soil heterogeneity in the Rheinbach-2 trial will enhance the significance of the results.

#### 4.5. Complementarity with Electromagnetic Induction

Other sensor technologies than GS rely on different signal sources and soil depths. Electromagnetic induction (EMI) integrates mainly clay and soil moisture content, but more soil properties such as bulk density have an influence on the EMI signal [46]. Multiple soil depths can be surveyed depending on the instrument [47]. Therefore, EMI is established as an appropriate tool to delineate field zones of plant growth and crop yield [22]. However, for some applications, influence of soil moisture during the survey or metallic field installations reduces EMI survey significance [42]. However, both soil texture and moisture together—mostly correlated because linked over the FC [21,44]—determine the EMI signal and cannot be separated without greater efforts. In contrast to EMI that captures proxies for soil properties, GS is considered a direct method [48]. In this respect, GS has advantages over EMI. First, GS is only to a minor degree influenced by soil moisture content if the survey is conducted at dry topsoil, because signal attenuation is known to be 1% per % soil moisture content and can, therefore, be corrected [5,17]. Second, GS allows direct derivation of soil texture as shown in this study. However, GS yields only soil information about approximately 0.3–0.5 m depth [48], while diverse EMI sensors capture different soil depths [47]. The combination of the advantages of GS and EMI is, therefore, probably the most promising [20].

## 5. Conclusions

Even within a distinct geopedological unit, differences in geology, mineralogy, and slope position impeded the universal use of a site-independent model for texture prediction based on on-the-go GS. Nevertheless, support to soil mapping and sampling was possible by detecting spatial soil heterogeneity. For such pattern recognition, data post-processing was dispensable. Case studies from field experimentation showed that on-the-go GS yields valuable information for optimised plot positioning and statistical evaluation. Site-specific, i.e., local calibrations, allowed quantitative predictions for single grain size fractions or entire texture classes. Prediction errors below 5% for single texture fractions were possible when the calibration data revealed sufficient texture variability. Quantitative texture data provided relevant input data for precision agriculture applications as shown in case studies for lime requirement and FC estimations. Such information can be used by users such as agricultural service providers.

The major obstacle for the widespread application—at least in a geologically diverse country—is the lack of a universal model. Still, advanced pedological-mineralogical knowledge is mandatory for representative reference sampling, model building, and interpretation of calibration and validation results. Creating a comprehensive spectral library for gamma spectrometry is desirable to enable universally (*sensu strictu*) valid calibration. Therefore, building such a database should include a standardisation for devices, spectra recording, calibration sample set, reference sampling and analyses, data processing, and evaluation. Once available, universal prediction models would be an important tool for agricultural service providers. This would mark a major step towards broad introduction into precision agriculture.

**Author Contributions:** Conceptualization: S.P. and T.W.H.; Methodology: T.W.H.; Investigation & Data Curation: T.W.H. and M.L.; Visualization: S.P. and T.W.H.; Writing: S.P., T.W.H. and M.L.; Project Administration and Funding Acquisition: S.P. All authors have read and agreed to the published version of the manuscript.

**Funding:** The study was funded by the German Federal Ministry of Education and Research (BMBF) within the BonaRes program, project I4S, subproject F (Grant No. 031B0513F).

**Acknowledgments:** We are grateful to Ralf Wehrle for English editing. Andreas Veller carefully conducted numerous texture analyses. Authorisation to access the fields and support by the private farmers is acknowledged.

**Conflicts of Interest:** The authors declare no conflict of interest. The funders had no role in the design of the study; in the collection, analyses, or interpretation of data; in the writing of the manuscript, or in the decision to publish the results.

## References

1. Kuang, B.; Mahmood, H.S.; Quraishi, M.Z.; Hoogmoed, W.B.; Mouazen, A.M.; van Henten, E.J. Sensing Soil Properties in the Laboratory, In Situ, and On-Line: A Review. *Adv. Agron.* **2012**, *114*, 155–223. [[CrossRef](#)]
2. Mahmood, H.S.; Hoogmoed, W.B.; van Henten, E.J. Proximal gamma-ray spectroscopy to predict soil properties using windows and full-spectrum analysis methods. *Sensors* **2013**, *13*, 16263–16280. [[CrossRef](#)]
3. Reinhardt, N.; Herrmann, L. Gamma-ray spectrometry as versatile tool in soil science: A critical review. *J. Plant Nutr. Soil Sci.* **2019**, *182*, 9–27. [[CrossRef](#)]
4. Cook, S.E.; Corner, R.J.; Groves, P.R.; Grealish, G.J. Use of airborne gamma radiometric data for soil mapping. *Aust. J. Soil Res.* **1996**, *34*, 183–194. [[CrossRef](#)]
5. IAEA, International Atomic Energy Agency. *Guidelines for Radioelement Mapping Using Gamma Ray Spectrometry Data*; IAEA-TECDOC-1363; IAEA: Vienna, Austria, 2003.
6. Megumi, K.; Mamuro, T. Concentration of uranium series nuclides in soil particles in relation to their size. *J. Geophys. Res.* **1977**, *82*, 353–356. [[CrossRef](#)]
7. Priori, S.; Bioanconi, N.; Costantini, E.A.C. Can  $\gamma$ -radiometrics predict soil textural data and stoniness in different parent materials? A comparison of two machine-learning methods. *Geoderma* **2014**, 226–227, 354–364. [[CrossRef](#)]
8. Heggemann, T.; Welp, G.; Amelung, W.; Angst, G.; Franz, S.O.; Koszinski, S.; Schmidt, K.; Pätzold, S. Proximal gamma-ray spectrometry for site-independent in situ prediction of soil texture on ten heterogeneous fields in Germany using support vector machines. *Soil Till. Res.* **2017**, 99–109. [[CrossRef](#)]
9. Stahr, K. Mineralbestand von Böden. In *Scheffer/Schachtschabel Lehrbuch der Bodenkunde*; Amelung, W., Blume, H.-P., Fleige, H., Horn, R., Kandeler, E., Kögel-Knabner, I., Kretschmar, R., Stahr, K., Wilke, B.-M., Eds.; Springer Spektrum: Berlin/Heidelberg, Germany, 2018; pp. 59–60.
10. Welp, G. Radionuklide. In *Scheffer/Schachtschabel Lehrbuch der Bodenkunde*; Amelung, W., Blume, H.-P., Fleige, H., Horn, R., Kandeler, E., Kögel-Knabner, I., Kretschmar, R., Stahr, K., Wilke, B.-M., Eds.; Springer Spektrum: Berlin/Heidelberg, Germany, 2018; pp. 614–622.
11. Wonik, T. Gamma-ray measurements in the Kirchrode I and II boreholes. *Palaeogeogr. Palaeoclimatol. Palaeoecol.* **2001**, *174*, 97–105. [[CrossRef](#)]
12. Piikki, K.; Söderström, M. Digital soil mapping of arable land in Sweden – Validation of performance at multiple scales. *Geoderma* **2019**, *352*, 342–350. [[CrossRef](#)]
13. van der Klooster, E.; van Egmond, F.M.; Sonneveld, M.P.W. Mapping soil clay contents in Dutch marine districts using gamma-ray spectrometry. *Europ. J. Soil Sci.* **2011**, *62*, 743–753. [[CrossRef](#)]
14. Petersen, H.; Wunderlich, T.; al Hagrey, S.A.; Rabbel, W. Characterization of some Middle European soil textures by gamma-spectrometry. *J. Plant Nutr. Soil Sci.* **2012**, *175*, 651–660. [[CrossRef](#)]
15. van Egmond, F.M.; Loonstra, E.H.; Limburg, J. Gamma ray sensor for topsoil mapping: The Mole. In *Proximal Soil Sensing*; Viscarra Rossel, R.A., McBratney, A.B., Minasny, B., Eds.; Springer: Dordrecht, The Netherlands; Heidelberg, Germany; London, UK; New York, NY, USA, 2010; pp. 323–332.
16. Loonstra, E.; van Egmond, F. On-the-go measurement of soil gamma radiation. In *Precision Agriculture – Papers Presented at the 7th European Conference on Precision Agriculture*; van Henten, E.J., Goense, D., Lokhorst, C., Eds.; Wageningen Academic Publishers: Wageningen, The Netherlands, 2009; pp. 415–422.
17. Gilmore, G. *Practical Gamma Ray Spectrometry*, 2nd ed.; repr. with corr.; Wiley: Chichester, UK, 2011; 387p.
18. Dickson, B.L.; Taylor, G.M. Quietening the noise: An evaluation of noise reduction methods applied to aerial gamma-ray survey data. *Explor. Geophys.* **2003**, *34*, 97–102. [[CrossRef](#)]
19. Pätzold, S.; Heggemann, T.; Welp, G.; Leenen, M. Small plot field experiments and proximal soil sensing (gamma and mid-infrared spectroscopy) provide reciprocal services. In Proceedings of the 12th European Conference on Precision Agriculture, Montpellier, France, 8–11 July 2019; pp. 146–147, (Book of Poster Abstracts). Available online: [http://ecpa2019.agrotic.org/wp-content/uploads/2019/07/ECPA2019\\_Proceedings\\_Poster.pdf](http://ecpa2019.agrotic.org/wp-content/uploads/2019/07/ECPA2019_Proceedings_Poster.pdf) (accessed on 4 February 2020).
20. Dennerley, C.; Huang, J.; Nielson, R.; Sefton, M.; Triantafilis, J. Identifying soil management zones in a sugarcane field using proximal sensed electromagnetic induction and gamma-ray spectrometry data. *Soil Use Manag.* **2018**, *34*, 219–235. [[CrossRef](#)]
21. Mertens, F.M.; Pätzold, S.; Welp, G. Spatial heterogeneity of soil properties and its mapping with apparent electrical conductivity. *J. Plant Nutr. Soil Sci.* **2008**, *171*, 146–154. [[CrossRef](#)]

22. Sun, Y.; Druecker, H.; Hartung, E.; Hueging, H.; Cheng, Q.; Zeng, Q.; Sheng, W.; Lin, J.; Roller, O.; Paetzold, S.; et al. Map-based investigation of soil physical conditions and crop yield using diverse sensor techniques. *Soil Till. Res.* **2011**, *112*, 149–158. [[CrossRef](#)]
23. Pätzold, S.; Hbirkou, C.; Dicke, D.; Gerhards, R.; Welp, G. Linking weed patterns with soil sensing data – a long-term case study. *Precis. Agric.* **2020**, *21*, 569–588. [[CrossRef](#)]
24. Sauer, D.; Felix-Henningsen, P. Saprolite, soils, and sediments in the Rhenish Massif as records of climate and landscape history. *Quatern. Int.* **2006**, *156*, 4–12. [[CrossRef](#)]
25. GD-NRW, Geologischer Dienst Nordrhein-Westfalen. *Bodenkarte zur Landwirtschaftlichen Standorterkundung 1:5000, m. Erl*; [Auszug aus dem digitalen Fachinformationssystem Bodenkunde], Verfahren Meckenheim-Rheinbach-Swisttal, LP (Landwirtschaft); Geologischer Dienst NRW: Krefeld, Germany, 2008; Available online: <https://www.geoportal.nrw/themenkarten> (accessed on 25 February 2020).
26. van Reeuwijk, L.P. *Procedures for Soil Analysis*; Technical paper No. 9; International Soil Reference and Information Centre: Wageningen, The Netherlands, 2002; Available online: <https://www.isric.org/explore/library> (accessed on 16 October 2019).
27. IUSS Working Group WRB. *World Reference Base for Soil Resources 2014, Update 2015*; International soil classification system for naming soils and creating legends for soil maps; World Soil Resources Reports No. 106; FAO: Rome, Italy, 2015; Available online: <http://www.fao.org/soils-portal/soil-survey/soil-classification/world-reference-base/en/> (accessed on 10 October 2019).
28. AG Boden, Ad-hoc-Arbeitsgruppe Boden. *Bodenkundliche Kartieranleitung*, 5th ed.; Schweizerbart'sche Verlagsbuchhandlung: Stuttgart, Germany, 2005; 438p.
29. VDLUFA, Verband der Landwirtschaftlichen Untersuchungs- und Forschungsanstalten. Bestimmung des Kalkbedarfs von Acker- und Grünlandböden. 2000. Available online: <https://www.vdlufa.de/Dokumente/Veroeffentlichungen/Standpunkte/0-9-kalk.pdf> (accessed on 25 November 2019).
30. Dickson, B.L.; Scott, K.M. Interpretation of aerial gamma-ray surveys—adding the geochemical factors. *AGSO J. Aust. Geol. Geophys.* **1997**, *17*, 187–200.
31. Wilford, J.R.; Bierwirth, P.N.; Craig, M.A. Application of airborne gamma-ray spectrometry in soil/regolith mapping and applied geomorphology. *AGSO J. Aust. Geol. Geophys.* **1997**, *17*, 201–216.
32. Meyer, W. *Geologie der Eifel*, 4th ed.; Schweizerbart'sche Verlagsbuchhandlung (Nägele u. Obermiller): Stuttgart, Germany, 2011; 704p.
33. Coulouma, G.; Caner, L.; Loonstra, E.H.; Lagacherie, P. Analysing the proximal gamma radiometry in contrasting Mediterranean landscapes: Towards a regional prediction of clay content. *Geoderma* **2016**, *266*, 127–135. [[CrossRef](#)]
34. Beceгато, V.A.; Beceгато, V.R.; Baum, C.A.; Lavnitcki, L.; Paulino, A.T. Multivariate statistical analysis correlating 238U, 232Th, and 40K equivalent activities in soil to geochemical data from an agricultural area. *J. Soils Sediments* **2019**, *19*, 1901–1910. [[CrossRef](#)]
35. Vos, C.; Don, A.; Prietz, R.; Heidkamp, A.; Freibauer, A. Field-based soil-texture estimates could replace laboratory analysis. *Geoderma* **2016**, *267*, 215–219. [[CrossRef](#)]
36. Stancu-Kristoff, G.; Vogel, A. Exkursion D—Zentrales Münsterland. In: *Exkursionsführer Jahrestagung 1989 in Münster. Mitteilungen der Deutschen Bodenkundlichen Gesellschaft* **58**, 259–315. Available online: [https://www.dbges.de/de/system/files/mitteilungen\\_dbg/MitteilungenderDBG1989\\_58.pdf](https://www.dbges.de/de/system/files/mitteilungen_dbg/MitteilungenderDBG1989_58.pdf) (accessed on 24 January 2020).
37. Mills, B.E.; Brorsen, B.W.; Arnall, D.B. The profitability of variable rate lime in wheat. *Precis. Agric.* **2019**. online first. [[CrossRef](#)]
38. Dordas, C. Role of nutrients in controlling plant diseases in sustainable agriculture. A review. *Agron. Sustain. Dev.* **2008**, *28*, 33–46. [[CrossRef](#)]
39. Leenen, M.; Welp, G.; Gebbers, R.; Pätzold, S. Rapid determination of lime requirement by mid-infrared spectroscopy: A promising approach for precision agriculture. *J. Plant Nutr. Soil Sci.* **2019**, *182*, 953–963. [[CrossRef](#)]
40. Vogel, S.; Gebbers, R.; Oertel, M.; Kramer, E. Evaluating Soil-Borne Causes of Biomass Variability in Grassland by Remote and Proximal Sensing. *Sensors* **2019**, *19*, 4593. [[CrossRef](#)]
41. Pätzold, S.; Leenen, M.; Frizen, P.; Heggemann, T.; Wagner, P.; Rodionov, A. Predicting plant available phosphorus using infrared spectroscopy with consideration for future mobile sensing applications in precision farming. *Precis. Agric.* **2019**. Online First. [[CrossRef](#)]

42. Hagverdi, A.; Leib, B.G. Site specific irrigation systems. In *Precision agriculture for sustainability*; Stafford, J., Ed.; Burleigh Dodds series in agricultural science 52; Burleigh Dodds Science Publishing: Cambridge, UK, 2019; pp. 323–346.
43. Bondesan, L.; Ortiz, B.V.; Morata, G.T.; Damianidis, D.; Jimenez, A.F.; Vellidis, A.F.; Morari, F. Evaluating and improving soil sensor-based variable irrigation scheduling on farmers' fields in Alabama. In *Precision Agriculture '19—Papers Presented at the 12th European Conference on Precision Agriculture*; Stafford, J., Ed.; Wageningen Academic Publishers: Wageningen, The Netherlands, 2009; pp. 649–664.
44. Hedley, C.B.; Yule, I.J. Soil water status mapping and two variable-rate irrigation scenarios. *Precis. Agric.* **2009**, *10*, 342–355. [[CrossRef](#)]
45. Hejcman, M.; Češková, M.; Schellberg, J.; Pätzold, S. The Rengen Grassland Experiment: Effect of Soil Chemical Properties on Biomass Production, Plant Species Composition and Species Richness. *Folia Geobot.* **2010**, *45*, 125–142. [[CrossRef](#)]
46. Heil, K.; Schmidhalter, U. The Application of EM38: Determination of Soil Parameters, Selection of Soil Sampling Points and Use in Agriculture and Archaeology. *Sensors* **2017**, *17*, 2540. [[CrossRef](#)]
47. Saey, T.; Simpson, D.; Vermeesch, H.; Cockx, L.; van Meirvenne, M. Comparing the EM38DD and DUALEM-21S Sensors for Depth-to-Clay Mapping. *Soil Sci. Soc. Am. J.* **2009**, *73*, 7–12. [[CrossRef](#)]
48. Gebbers, R. Proximal soil surveying and monitoring techniques. In *Precision Agriculture for Sustainability*; Stafford, J., Ed.; Burleigh Dodds series in agricultural science 52; Burleigh Dodds Science Publishing: Cambridge, UK, 2019; pp. 29–78.



© 2020 by the authors. Licensee MDPI, Basel, Switzerland. This article is an open access article distributed under the terms and conditions of the Creative Commons Attribution (CC BY) license (<http://creativecommons.org/licenses/by/4.0/>).